Int J Adv Manuf Technol (2017) 92:497–504
DOI 10.1007/s00170-017-0172-x

ORIGINAL ARTICLE

Numerical simulation and experimental study on the non-axisymmetric die-less shear spinning

Z. Jia[1] **· Z. R. Han**[1] **· B. M. Liu**[1] **· Z. J. Fan**[1]

Received: 20 October 2016 / Accepted: 15 February 2017 / Published online: 27 February 2017

Abstract The non-axisymmetric cone has broad application prospects and is feasible to be manufactured via die-less shear spinning process which however lacks of research. With the roller path equation and other boundary conditions, the finite element model for non-axisymmetric die-less shear spinning process is established and simulated by adopting ABAQUS/explicit software in this study. The FEM results are experimentally verified by comparing the morphology and the HCAs. The distribution of stress and strain in different working conditions and the ellipticity and the elongation of the material in different spinning process during non-axisymmetric die-less shear spinning process are analyzed. It shows that the 0° area of the flange is the position where the wrinkle occurs easily, and the elongation of the material reaches the maximum value; the larger equivalent stress and strain distribute on the conical surface with the smaller HCA. With the movement of the roller, the ellipticity of the cross section increases in the bigger HCA working conditions, but decreases in the smaller HCA working conditions due to the combined effects of the deformation and the springback.

Keywords Non-axisymmetric spinning · Die-less · Fem · Half cone angle

✉ Z. R. Han
hanren888@163.com

[1] Key Lab of Fundamental Science for National Defense of Aeronautical Digital Manufacturing Process, Shenyang Aerospace University, 37 Daoyi South Avenue, Daoyi Development District, Shenyang 110136, China

1 Introduction

The hollow cone parts, such as air compressor, lampshade, and hopper (as shown in Fig. 1), are widely used in the fields of aerospace, auto car, agricultural machinery, and so on [1–3]. Due to the high ratio of the height to the diameter, it is difficult to produce the hollow cone parts through deep drawing [4]. Spinning technique, an incremental forming technology, has thus been a very attractive area of research [5–7]. With the in-depth study, non-circular spinning is also derived besides the conventional ones. An ellipse spinning is successfully tried with a new device designed by Gao et al. [8]. An asymmetric truncated-elliptical-cone-shaped product is obtained from a 1-mm-thick aluminum sheet by developing the synchronous spinning machine [9]. The triangular cross section spinning is carried out by Lai et al. [10, 11], and the force in the spinning process is analyzed. In the above investigations of non-circular spinning, the mandrel whose shape is in accordance with the cone is used. If the parameters of the part are changed, the mandrel has to be amended, which will cause not only the increase of the cost but also the decrease of the flexibility.

In recent years, the spinning flexibility has been enhanced, and the die-less spinning is proposed to form the hollow parts without a consistent shape mandrel by using the high stiffness blank of the workpiece [12, 13]. Based on that, non-axisymmetric cone or tubal parts for special purpose is processed by the die-less spinning, and the advantage of its flexibility is further reflected. Xia et al. [14–17] investigated the non-axisymmetric spinning of the tube blanks and proposed a novel spinning process, in which the blank does not rotate but only moves in straight lines. Then the process of the multi-pass offset-tube neck-spinning is simulated through the MARC software, and the optimization parameters for offset and oblique tubes spinning are obtained. It shows that the distribution of strain and stress is non-axisymmetric; the ellipticity and the axial

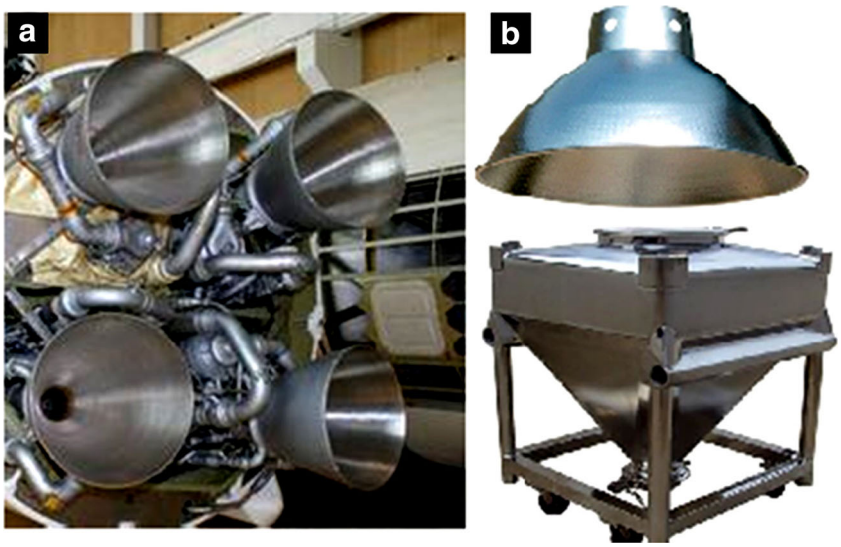

Fig. 1 Shell parts with cone shape of **a** air compressor and **b** lampshade and hopper

elongation of the spun workpiece increase with the increase of the spinning passes; the spinning force varies periodically with the revolution angle of the roller around the blank, and the force during the backward path spinning is greater than that during the forward path spinning. However, the forming mechanism of the non-axisymmetric spinning of tube parts is quite different from the one of the sheet blank. For example, the cone shape cannot be formed with an irrational sheet blank.

Up to date, although much work has been done on the non-axisymmetric spinning with the tubular blank, there is little research about the shear die-less ones. In our previous research [18], the roller path for the non-axisymmetric spinning and the wall thickness distribution of the spun workpiece with the half cone angles (HCAs) of 30–45° were studied. It was found that the wall thicknesses of the oblique cone after spinning have the trend of the sine law according to their corresponding HCAs. So the non-axisymmetric spinning can be considered as the shear one. But the research only involved the working condition with the HCA ranging from 30 to 45°, and the metal rheological behavior, which was related to the deformation mechanism, was not investigated. Therefore, the finite element modeling (FEM), combining with the experimental verification, is adopted to investigate the basic theory of the non-axisymmetric die-less shear spinning in this paper.

2 Finite element model

2.1 Non-axisymmetric roller path

The two HCAs of the non-axisymmetric cone are different when being viewed from the side, the cone also can be considered as the assemblage of many eccentric circle cross sections, as shown in Fig. 2. Due to its geometry characteristic, the non-axisymmetric cone cannot be formed through the simple roller path of a straight line. The roller needs to move along a reciprocated and calculated track.

Fig. 3 shows assembly drawing of the roller, the spindle, and the disk blank. The schematic diagram of the roller path in 360° rotated by the spindle is illustrated in Fig. 4. The forming principle of the non-axisymmetric cone by the die-less spinning is that the roller reciprocates on the radial direction (Coordinate axis X) cooperating with the small axial (Coordinate axis Z) movement of it and the rotation of the workpiece. The synthesis of the whole movement relationship displays as a helical line with the eccentric circle cross section, and the movement relationship is given by [18]

$$L_i = e_i\cos(180-\theta_i) + \sqrt{e_i^2\cos^2(180-\theta_i) + r_i^2 - e_i^2} \tag{1}$$

Where, L_i is the rotation radius when the workpiece rotates the angle θ_i; r_i, and e_i are the radius and the eccentricity of the new cross-section circle to the initial one when the workpiece rotates the angle θ_i. They can be calculated by the following equations:

$$r_i = \frac{h_i \Big/ \tan\alpha + h_i \Big/ \tan\gamma + 2r_0}{2} \tag{2}$$

$$e_i = \frac{h_i \Big/ \tan\alpha - h_i \Big/ \tan\gamma}{2} \tag{3}$$

$$\theta_i = \frac{360st_i}{60} = 60st_i \tag{4}$$

where r_0 is the radius of the initial cross section; h_i is the height of the cone when the workpiece rotates the angle θ_i; t_i is the time of the workpiece rotates the angle θ_i; α and γ are the HCAs when being viewed from the side.

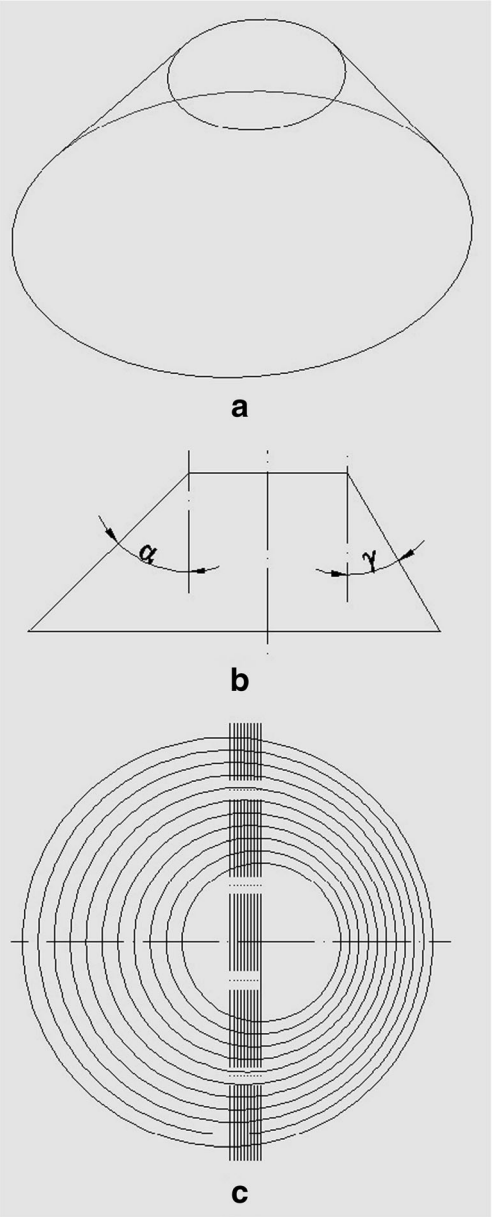

Fig. 2 **a** stereo, **b** side, and **c** top views of non-axisymmetric cone

With the geometry conditions r_0, α, and γ and the step conditions h_i and t_i, the roller path used in the FEM and the experiment can be obtained.

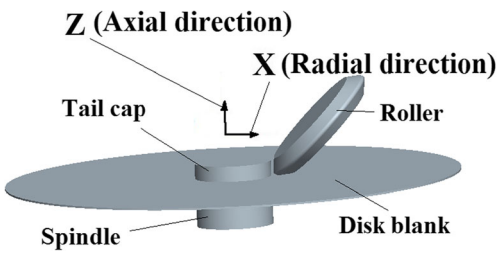

Fig. 3 Assembly drawing of the non-axisymmetric spinning

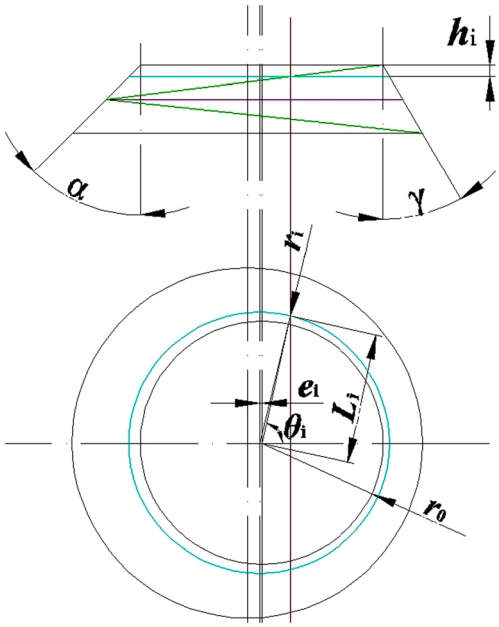

Fig. 4 Schematic diagram of the roller path in 360° rotated by the spindle

2.2 Other boundary conditions

The 3D geometric models of the roller, the spindle, and the disk blank for the non-axisymmetric spinning are imported and assembled in the ABAQUS software. The disk blank is defined as a 3D deformable solid body, meshed using C3D8R elements for "8-node linear brick, and reduced integration and hourglass control". The rigid bodies are assigned to the roller, the spindle, and the tail cap. The roller can move along the radial and axial direction and rotate around its central axis freely. The diameter of the roller is 110 mm, with the working radius of 2 mm. The inclination angle of the roller to the axial direction is 45°. According to the production experience, the friction coefficient is set to 0.4 when no lubrication is used among the tail cap, disk blank, and spindle, and the friction coefficient is 0.15when the lubrication of oil is used between the roller and the disk blank. The roller can be rotated by the workpiece due to the friction. The material of the blank, used in this work, is 6061 aluminum alloy (annealed). The diameter and thickness are 260 and 1.2 mm, respectively. The constitutive equation is obtained from Ref. [13]:

$$\sigma = 234\varepsilon^{0.26} \tag{5}$$

where σ is the true stress; ε is the true strain. The mechanical properties of the alloy are shown in Table 1.

With the boundary conditions, the finite element model for the non-axisymmetric spinning is established and simulated through the dynamic explicit module of ABAQUS.

Table 1 Mechanical properties of 6061 aluminum alloy (annealed)

Symbol	Definition	Value	Unit
E	Elastic modulus	67,308	MPa
υ	Poisson's ratio	0.33	–
σ_s	Yield strength	51.59	MPa
σ_b	Tensile strength	146.12	MPa
δ	Elongation	30	%

Table 2 Working conditions of the FEM

HCA	Working condition I	Working condition II	Working condition III
α (°)	45	60	60
γ (°)	30	30	45

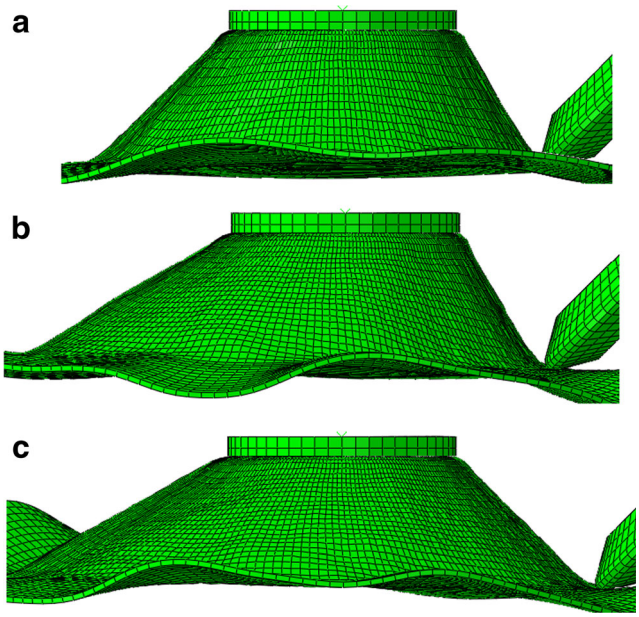

Fig. 5 FEM results with the Working condition of **a** I, **b** II, and **c** III

3 Simulation results and discussion

3.1 Simulation results and experimental verification

In order to investigate the effects of HCAs on the metal flow of the non-axisymmetric die-less spinning, three combinations of the HCAs, namely 30, 45, and 60°, are selected. The total axial feeding distance of the roller path is 50 mm. The calculations are carried out according to the working conditions in Table 2, and the results are shown in Fig. 5. In order to verify the simulation results, the non-axisymmetric spinning experiment is carried out using the PS-CNCSXY 5-axis spinning machine with the same working conditions. The feed speed of the roller is 5000 mm/min; the fillet radius of the roller is 2 mm. During the spinning process, the spindle speed determines the rotate angle θ_i; it must match the radial and axial movement of the roller, as well as the relationship shown in eq. (1). So the feed rate and the spindle speed depend on the feed speed, and the matching relationship between the rotational velocity of the workpiece and the movement of the roller are carried out by the numerical control system of the spinning machine. Other processing parameters adopted in the experiment are the same as those adopted in the simulation. The experiment results are shown in Fig. 6.

The morphology of the workpiece under the Working condition I is shown in Fig. 7. It shows that both the workpieces from experiment and FEM exhibit non-axisymmetric cone shape, and all the HCAs from the three working conditions are contrasted in Fig. 8. The maximum deviation of the HCAs between the experiments and the simulation results is 10.9%. Moreover, the wall thicknesses on the direction of α and γ of HCA are measured and calculated, as shown in Fig. 12. There are six measuring positions on each HCA direction and distributed evenly axially. The maximum deviation of wall thickness is within 15.1%. It indicates that the FEM describes the non-axisymmetric die-less shear spinning well.

3.2 Discussion of simulation results

3.2.1 Analysis of deformation process

The deformation result in the spinning process of Working condition I is shown in Fig. 9. It obviously shows that the

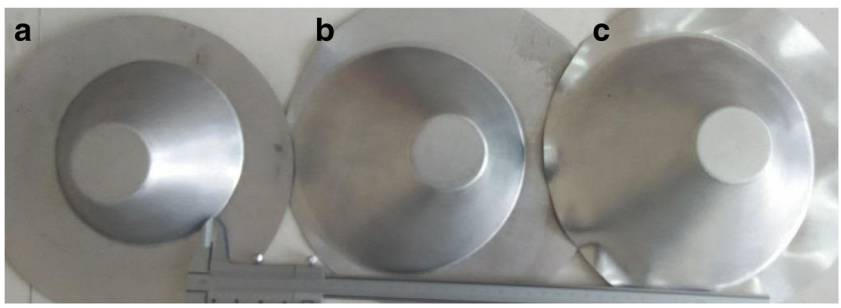

Fig. 6 Experimental results with the Working condition of **a** I, **b** II, and **c** III

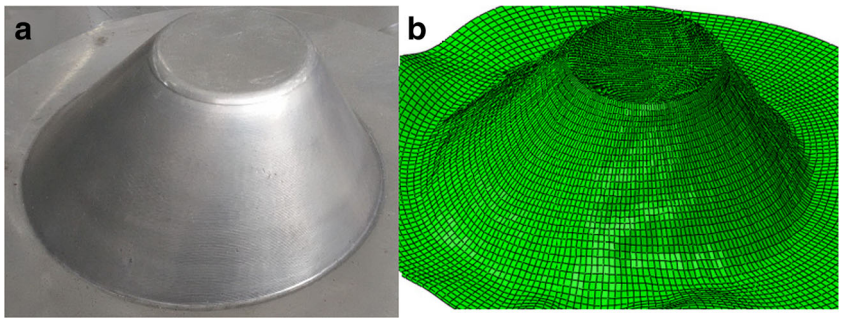

Fig. 7 Morphology of the workpiece obtained from **a** experiment and **b** FEM

eccentricity enlarges gradually with the increase of the rotation rounds; the elongation of the deformed material along the conical slope direction is non-axisymmetric; the elongation at 0° area where the biggest HCA locates is significantly greater than that at 180° area where the smallest HCA locates.

The diameter of the workpiece at the spinning area increases gradually with the spinning process ongoing (see Fig. 9a, b, c). Due to the increasing of the eccentricity and the diameter, the flange of the blank left at the 0° area is significantly smaller than that at 180° area, and it is easier to wrinkle on the flange which is not left enough to restrain the uneven stress. Furthermore, the elongation of the material reaches the maximum value at 0° area and the minimum value at 180° area, and the difference between them grows up with the roller moving deeper along the axial direction.

3.2.2 Stress and strain fields of different working conditions

Fig. 10 shows the distribution of the equivalent stress after 70 s during the spinning process. It can be found that the larger equivalent stress distributes on the conical surface with the smaller HCA. The distribution of the equivalent stress in the Working condition II is thus the most uneven due to the largest difference between its HCAs. When the working condition is fixed, the equivalent stress reaches maximum value at the position where the conical surface with the smaller HCA connects to the flange of the blank.

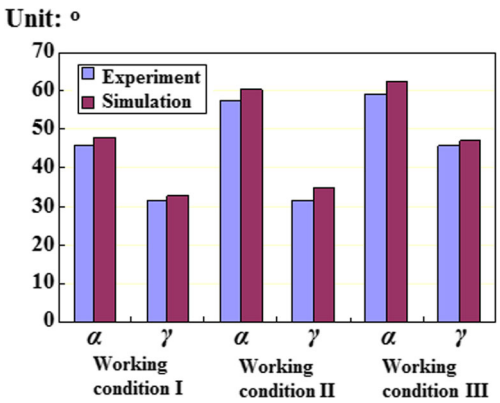

Fig. 8 Contrasts of the HCAs

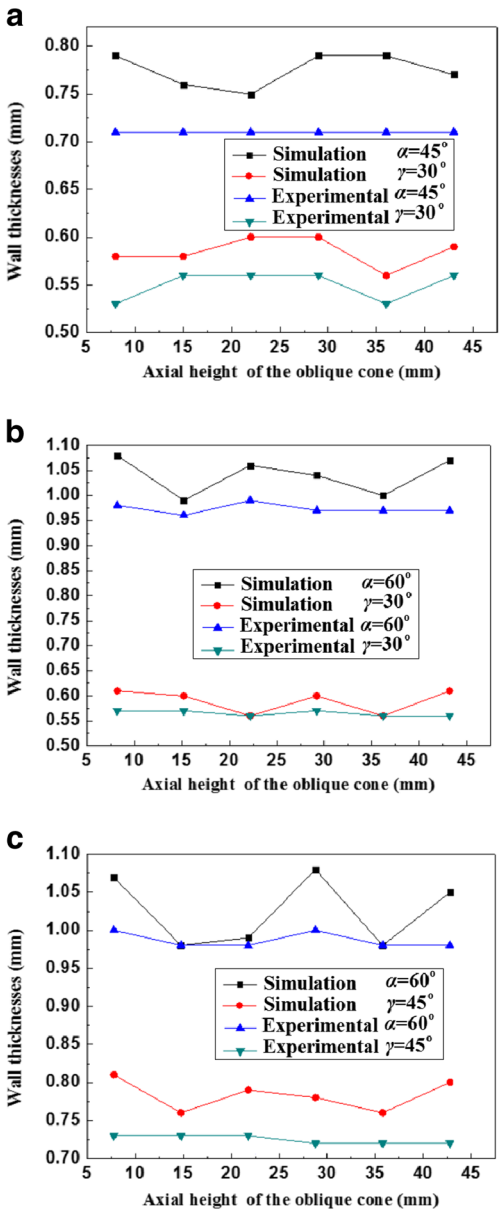

Fig. 12 Wall thickness distributions of the working conditions of **a** I, **b** II, and **c** III

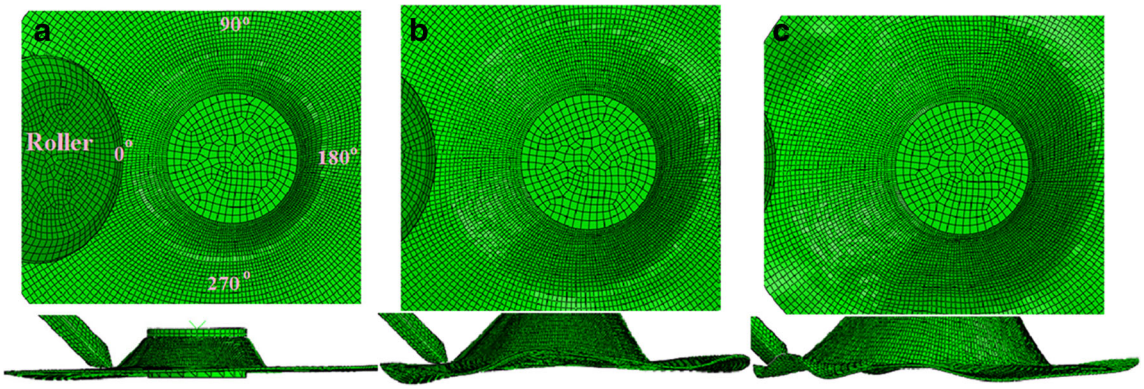

Fig. 9 Deformation process of the non-axisymmetric spinning with working condition I after the time of (**a**) 33 s, (**b**) 71 s, and (**c**) 100 s

Fig. 11 shows the distribution of the equivalent strain after 70 s during the spinning process. It shows that the larger HCA conical surface is formed with the smaller equivalent strain distribution, and this result meets well with the conclusion of Ref. [17] that the wall thickness distribution of non-axisymmetric shear spinning accords with the sine law. It also means that the bigger wall thickness thinning occurs in the case of the smaller HCA. Although the metal of the conical wall with the bigger HCA is stretched longer, the larger total deformation happens to the smaller HCA wall. It indicates that the thinning of the wall thickness is the main deformation for the non-axisymmetric shear spinning. The largest deformation distributes at the slope but not the bottom of the cone which has the smallest HCA. Hence, the deformation distribution of Working condition II is the most uneven due to the largest HCA difference.

3.2.3 Wall thickness distributions of different working conditions

The wall thickness distributions of the three working conditions are shown in Fig. 12. It can be found that, the wall thickness with a smaller HCA gets thinner, and this is consistent with the analysis of the strain field. Besides that, the thinning trend of the wall thickness abides by the sine law, which confirms our previous conclusion that the non-axisymmetric die-less spinning can be considered as a shear one.

3.2.4 Ellipticity of different working conditions

Due to the complexity of the non-axisymmetric spinning process, the geometric error—ovalization will happen onto the eccentric cross sections inevitably. The difference between the maximum and minimum diameter in the same cross-section of the workpiece can be defined as the ellipticity e [19]:

$$e = \frac{2(D_{\max} - D_{\min})}{D_{\max} + D_{\min}} \times 100\% \tag{6}$$

e is an important index to evaluate the forming quality of the workpiece by the die-less spinning. The mating accuracy of the workpiece between parts is determined by its value. Fig. 13 shows the ellipticity e along the axial (direction Z) direction of the three working conditions in different spinning passes. It shows that the e in the small HCA working condition is smaller than the one in the big working condition. The ellipticity increases with the marching of the spinning process in the bigger HCA working conditions, but decreases slightly in the smaller one. This is mainly because that the radial feed of the roller is bigger with the smaller HCA. Therefore, when the roller goes down along the axial direction (direction Z), the upper cross section which has been formed will be affected by the

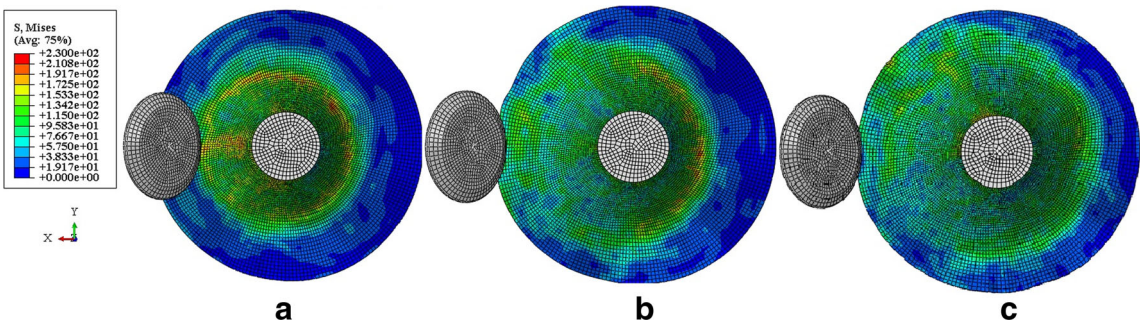

Fig. 10 Equivalent stress fields of the working conditions of **a** I, **b** II, and **c** III. The unit of stress is in MPa

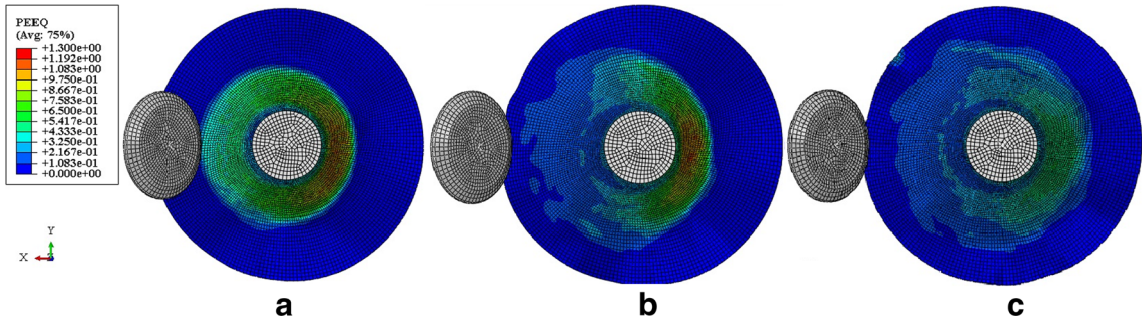

Fig. 11 Equivalent strain fields of the working conditions of **a** I, **b** II, and **c** III

subsequent deformation more easily, and the lower section will suffer smaller effect of the subsequent deformation. Although, the effect of the deformation on the circularity of the cross section in the larger HCA working conditions is smaller, it suffers springback more seriously. With going deeper along the axial direction, the rest of the blank flange disappears gradually, and its constraint on the springback drops rapidly in the bigger HCA working conditions. The uneven springback destroys the roundness of the cross section. So the *e* of Working condition II and III grows up along the axial direction.

4 Conclusions

(1) With the roller path equation, the non-axisymmetric die-less shear spinning process is simulated by the 3D elasto-plastic finite element model. The FEM results are verified experimentally.

(2) The edge of the blank flange is easier to wrinkle at the 0° area which is the bottom of the conical wall with the bigger HCA due to the lack of the flange to restrain the uneven stress. Furthermore, the elongation of the material reaches the maximum value at 0° area and the minimum value at 180° area.

(3) The distributions of the equivalent stress and strain on the workpiece formed by non-axisymmetric die-less spinning are uneven. The larger value distributes on the conical surface with the smaller HCA.

(4) The ellipticity of the cross section increases with the marching of the spinning process in bigger HCA working conditions, but decreases slightly in the smaller HCA working conditions due to the combined effects of the deformation and the springback.

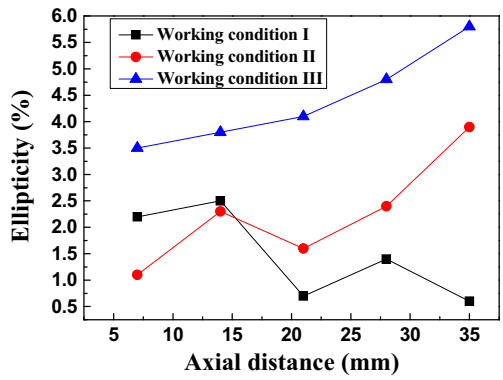

Fig. 13 Ellipticity of the three working conditions

Acknowledgements This work was financially supported by the Natural Science Foundation of Liaoning Province, China (No. 201602558), and authors wish to express their gratitude.

References

1. Xia Q, Xiao G, Long H, Cheng X, Shen X (2014) A review of process advancement of novel metal spinning. Int J Mach Tools Manuf 85(7):100–121
2. Zhan M, Yang H, Guo J, Wang XX (2015) Review on hot spinning for difficult-to-deform lightweight metals. Trans Nonferrous Metals Soc China 25(6):1732–1743
3. Kwiatkowski L, Melsheimer O, Wenzel S, Kunert J, Tekkaya AE (2010) Experimental investigation of tool path strategies for incremental necking-in. Int J Mater Form 3(3):967–970
4. Zhao Y (2005) Present situation of spinning technology. Forging and stamping Technol 30(5):95–97 (in Chinese)
5. Zeng R, Ma F, Liang H, Jianjun L (2015) Investigation on spinnability of profiled power spinning of aluminum alloy. Int J Adv Manuf Technol 80(1):535–548
6. Jiang SY, Zheng YF, Ren ZY, Li CF (2009) Multi-pass spinning of thin-walled tubular part with longitudinal inner ribs. Trans Nonferrous Metals Soc China 19(1):215–221
7. Li Y, Wang J, Lu GD, Pan GL (2014) A numerical study of the effects of roller paths on dimensional precision in die-less spinning of sheet metal. J Zhejiang University Sci A 15(6):432–446
8. Gao XC, Kang DC, Meng XF, Wu HJ (1999) Experimental research on a new technology–ellipse spinning. J Mater Process Technol 94(2):197–200
9. Shimizu I (2010) Asymmetric forming of aluminum sheets by synchronous spinning. J Mater Process Technol 210(4):585–592
10. Xia QX, Lai ZY, Long H, Chen XQ (2013) A study of the spinning force of hollow parts with triangular cross sections. Int J Adv Manuf Technol 68(9–12):2461–2470
11. Lai ZY, Xia QX, Xu T, Cheng XQ (2011) Strain grid experiment of spinning of hollow part with triangular arc-type cross-section. J South China University of Technol 39(8):7–12 (in Chinese)

12. Sekiguchi A, Arai H (2012) Control of wall thickness distribution by oblique shear spinning methods. J Mater Process Technol 212(4):786–793
13. Han ZR, Fan ZJ, Xiao Y, Jia Z (2016) Research on thickness distribution of oblique cone in dieless shear spinning. doi:10.1007/s00170-016-9565-5Int J Adv Manuf Technol
14. Xia QX, Xie SW, Huo YL, Ruan F (2008) Numerical simulation and experimental research on the multi-pass neck-spinning of non-axisymmetric offset tube. J Mater Process Technol 206(1):500–508
15. Xia QX, Cheng XQ, Hu Y, Ruan F (2006) Finite element simulation and experimental investigation on the forming forces of 3D non-axisymmetrical tubes spinning. Int J Mech Sci 48(7):726–735
16. Xia Q (2004) Investigation on the mechanism of the spinning technology of the 3D non-axisymmetric parts. Chinese J Mech Eng 40(2):153–156 (in Chinese)
17. Cheng X, Feng W, Xia Q (2008) The study on the numerical simulation of non-axisymmetric tube neck-spinning and process parameters optimization. J plasticity engineering 15(4):61–66 (in Chinese)
18. Han Z, Xu Q, Jia Z, Li X (2015) Experimental research on oblique cone die-less shear spinning. Proceedings of the Institution of Mechanical Engineers Part B J Eng Manuf 78(23):11772–11782
19. Ding W, Zhang K, Yang C, Hu Z (2010) Study on the ovality of hollow shafts with equal inner diameter formed by CROSS wedge rolling. J Plasticity Eng 17(3):27–31 (in Chinese)